Biochimica et Biophysica Acta 1827 (2013) 1213–1225

Contents lists available at ScienceDirect

Biochimica et Biophysica Acta

journal homepage: www.elsevier.com/locate/bbabio

High resolution respirometry analysis of polyethylenimine-mediated mitochondrial energy crisis and cellular stress: Mitochondrial proton leak and inhibition of the electron transport system

Arnaldur Hall [a,b], Anna K. Larsen [a,b], Ladan Parhamifar [a,b], Kathrine D. Meyle [a], Lin-Ping Wu [a,b], S. Moein Moghimi [a,b,*]

[a] Centre for Pharmaceutical Nanotechnology and Nanotoxicology, University of Copenhagen, Universitetsparken 2, DK-2100 Copenhagen Ø, Denmark
[b] NanoScience Centre, University of Copenhagen, DK-2100 Copenhagen Ø, Denmark

ARTICLE INFO

Article history:
Received 8 April 2013
Received in revised form 7 June 2013
Accepted 2 July 2013
Available online 11 July 2013

Keywords:
Cell death
Cytochrome *c* oxidase
Electron transport system
Mitochondrial membrane potential
Mitochondrial uncoupling
Polyethylenimine

ABSTRACT

Polyethylenimines (PEIs) are highly efficient non-viral transfectants, but can induce cell death through poorly understood necrotic and apoptotic processes as well as autophagy. Through high resolution respirometry studies in H1299 cells we demonstrate that the 25 kDa branched polyethylenimine (25k-PEI-B), in a concentration and time-dependent manner, facilitates mitochondrial proton leak and inhibits the electron transport system. These events were associated with gradual reduction of the mitochondrial membrane potential and mitochondrial ATP synthesis. The intracellular ATP levels further declined as a consequence of PEI-mediated plasma membrane damage and subsequent ATP leakage to the extracellular medium. Studies with freshly isolated mouse liver mitochondria corroborated with bioenergetic findings and demonstrated parallel polycation concentration- and time-dependent changes in state 2 and state 4o oxygen flux as well as lowered ADP phosphorylation (state 3) and mitochondrial ATP synthesis. Polycation-mediated reduction of electron transport system activity was further demonstrated in 'broken mitochondria' (freeze-thawed mitochondrial preparations). Moreover, by using both high-resolution respirometry and spectrophotometry analysis of cytochrome *c* oxidase activity we were able to identify complex IV (cytochrome *c* oxidase) as a likely specific site of PEI mediated inhibition within the electron transport system. Unraveling the mechanisms of PEI-mediated mitochondrial energy crisis is central for combinatorial design of safer polymeric non-viral gene delivery systems.

1. Introduction

Synthetic polycations have gained increasing attention as non-viral delivery systems for nucleic acid therapeutics [1–3]. Polycations such as polyethylenimines (PEIs) and their derivatives are effective transfection reagents by their capacity to compact nucleic acids into polyplexes, thereby protecting the nucleic acids from degradation, as well as promoting their successful delivery into a wide range of cells [1,3–8]. The majority of polyplexes enter cells via clathrin-mediated endocytosis, but there are many other suggested internalization mechanisms, including caveolae-mediated pathways as well as internalization through polycation-mediated plasma membrane perturbation/destabilization processes [3,9–14]. Despite the fact that synthetic polycations are effective non-viral candidates, it is of great concern that the polycations showing the best transfection efficiency, typically also display higher cytotoxicity [3,4,9–11].

PEIs are the best investigated polycationic vectors existing in both linear and branched morphology [3,15]. The 25 kDa branched PEI (25k-PEI-B) is among the most efficient polycationic transfection agents, but also induces severe cytotoxicity in clinically relevant human cell lines [10]. Accordingly, there have been numerous empirical and combinatorial approaches to lessen PEI-induced cytotoxicity. Some of these modifications have reduced cytotoxicity, but at the expense of poor transfection efficacy and low duration period-specific gene expression or silencing; however, in most cases cytotoxicity still persists when examined closely [3,4]. The underlying mechanisms of PEI-induced cytotoxicity are complex, multifaceted and not fully understood. A number of studies have shown that PEI can induce

Abbreviations: Anti-A, antimycin A; Asc, ascorbate; NaN_3, sodium azide; CCCP, carbonyl cyanide m-chlorophenylhydrazone; CI, complex I; CII, complex II; CIII, complex III; CIV, complex IV; cyt *c*, cytochrome *c*; DIC, differential interference contrast; ETS, electron transport system; RFRs, respiratory flux ratios; FBS, fetal bovine serum; L, LEAK respiration; (L/E), LEAK control ratio; Mna, malonic acid; MTG, MitoTracker Green; ((R-L)/E), netROUTINE control ratio; NADH, nicotinamide adenine dinucleotide; OXPHOS, oxidative phosphorylation; PEI, polyethylenimine; PI, propidium iodide; RCR, respiratory control ratio; (R/E), ROUTINE control ratio; R, ROUTINE respiration; Rote, rotenone; ROX, residual oxygen consumption; TMPD, *N,N,N′,N′*-tetramethyl-*p*-phenylenediamine; TMRM, tetramethyl rhodamine methyl ester

* Corresponding author at: Centre for Pharmaceutical Nanotechnology and Nanotoxicology, University of Copenhagen, Universitetsparken 2, DK-2100 Copenhagen Ø, Denmark. Tel.: +45 35336528.
E-mail addresses: imedicine.moghimi@outlook.com, moien.moghimi@sund.ku.dk (S.M. Moghimi).

0005-2728/$ – see front matter © 2013 Elsevier B.V. All rights reserved.
http://dx.doi.org/10.1016/j.bbabio.2013.07.001

cell death through multiple pathways (e.g., necrosis, apoptosis and autophagy) with mitochondrial involvement [9,11,16–18]. Indeed, mitochondria play a vital role in cellular energy metabolism and the mitochondrial membrane potential ($\Delta\psi_m$) is a key indicator of cell viability; loss of $\Delta\psi_m$ is associated with cellular stress and cell death, and dissipation of $\Delta\psi_m$ may promote apoptosis [19]. The $\Delta\psi_m$ is generated from the build-up of proton-driven electrochemical gradient across the inner mitochondrial membrane, as a result of the activity of the protein complexes of the electron transport system (ETS) and the integrity of the mitochondrial inner membrane [20,21]. Electrons that originate from the oxidation of reduced nicotinamide adenine dinucleotide (NADH) by complex I (NADH-ubiquinone oxidoreductase; CI), and from oxidation of succinate by complex II (succinate-ubiquinone oxidoreductase; CII), flow through the electron transport system with molecular oxygen being the final electron acceptor [22]. Electron transport through the ETS is coupled with proton translocation by the inner membrane complexes I, III (ubiquinol-cytochrome *c* oxidoreductase; CIII) and IV (cytochrome *c* oxidase; CIV). This activity generates the electrochemical proton gradient, which is utilized by the mitochondrial F_0/F_1-ATP synthase to produce ATP [20,23]. The proton pumps of the electron transport system, together with the ATP synthase, create a proton circuit across the inner membrane, which is central to mitochondrial bioenergetics and cellular homeostasis [20–24]. This integrated process of mitochondrial respiration is referred to as oxidative phosphorylation (OXPHOS) and the inability of mitochondria to sufficiently produce ATP can lead to energy depletion and cellular stress, and may induce cell death through different pathways [25–29].

Earlier studies have shown that exposure of various human cell lines to PEI and PEI/DNA complexes initiates loss of $\Delta\psi_m$ [10] as well as cytochrome *c* (cyt *c*) release from the mitochondrial intermembrane space [9,11]. Furthermore, studies with isolated mitochondria have demonstrated PEI-mediated inhibition of respiration, dissipation of $\Delta\psi_m$ and large amplitude osmotic swelling [30]. These observations strongly indicate that cytoplasmic PEI may perturb mitochondrial membranes and interfere with electron transport processes. Accordingly, we have now examined the effect of 25k-PEI-B on bioenergetic processes with a specific focus on mitochondrial proton leak and ETS capacity in H1299 cell line as well as in freshly isolated mouse liver mitochondria and 'broken mitochondria' (freeze-thawed mitochondrial preparations). A better understanding of these events could open the path for designing safer polymers through combinatorial approaches for transfection purposes and achieving clinically acceptable duration period-specific gene expression or silencing.

2. Materials and methods

2.1. Materials

The 25k-PEI-B (dissolved in milli-Q H_2O) and cyt *c* oxidase assay kit were purchased from Sigma-Aldrich (Denmark). The ATPlite luminescence assay system was purchased from Perkin Elmer (Skovlunde, Denmark). Hoechst-33342, MitoTracker Green (MTG), propidium iodide (PI) and tetramethyl rhodamine methyl ester (TMRM) were purchased from Life Technologies Europe BV (Denmark). All other materials were purchased from Sigma-Aldrich (Denmark).

2.2. Cell culture

H1299 cells (ATCC number: CRL-5803; Sigma-Aldrich) were cultured in RPMI-1640 medium at 37 °C with 0.1 mg/mL penicillin/streptomycin, 2 mM L-Glutamine and 10% FBS in 21% O_2 and 5% CO_2. Cells were harvested at 80–90% confluence and not allowed to exceed 12 passages. Experiments pertaining to H1299 cells were performed at 60–70% confluence.

2.3. Live cell imaging and measurements of mitochondrial membrane potential in H1299 cells

H1299 cells were seeded (8.0×10^4 cells/well) in 200 μL in μ-slide 8 well-plates (Ibidi, Denmark). Cells were grown to 60–70% confluency and thereafter stained with the mitochondrial dyes MTG (300 nM) and TMRM (200 nM) as well as with the nuclear dye Hoechst-33342 (5 μg/mL) for 20 min at 37 °C. MTG accumulates into polarized mitochondria and binds covalently to intramitochondrial protein thiols where it remains bound after depolarization, whereas TMRM accumulates in a $\Delta\psi_m$-dependent manner and leaks out of mitochondria after reduction in $\Delta\psi_m$ [31–34]. After staining, cells were washed twice and subjected to 10 μg/mL 25k-PEI-B in growth medium at 37 °C followed by live cell imaging. Imaging was performed on a Leica AF6000LX microscope equipped with a 63× (numerical aperture = 1.47) oil objective using 1.6× magnification. Images were acquired with appropriate red (excitation with band pass = 555/25 nm, emission with band pass = 605/52 nm), green (excitation with band pass = 470/40 nm, emission with band pass = 525/50 nm) and blue (excitation with band pass = 360/40 nm, emission with band pass = 470/40 nm) filters, respectively. In addition, differential interference contrast (DIC) images were taken simultaneously to visualize morphological changes. Z-stacking was performed using appropriate sectioning steps. Alterations of TMRM and MTG fluorescence intensity were quantified with FACS (BD FACS Array™ Cell Analysis) (10,000 events were counted) at different time intervals of PEI exposure. Cell viability was followed by FACS and microscopy. Briefly, cells were stained with the nuclear dye Hoechst-33342 (1 μg/mL, 15 min, 37 °C) and washed twice and stained with 1 μg/mL PI for 10 min at 37 °C. Cells were then incubated with 10 μg/mL 25k-PEI-B for 90 min at 37 °C before analysis.

2.4. Isolation of mouse liver mitochondria

Mouse liver mitochondria were isolated from young female NMRI mice (approximately 8–12 weeks old and 35–40 g in body weight). All animals used in this study were housed in a light/dark phase cycle of 12 h with free access to food and water. The animals were killed by cervical dislocation and the liver was rapidly removed, rinsed and minced with scissors, in ice-cold isolation medium (mannitol 225 mM, sucrose 75 mM, Tris–HCl 5 mM, EGTA 0.1 mM and BSA 5 mg/mL, pH 7.0). The liver was subsequently homogenized in a Potter–Elvehjem glass homogenizer using a motor-driven Teflon-pestle. The liver homogenate was centrifuged for 5 min at 800 ×*g*, the supernatant was decanted and the centrifugation step was repeated again. The supernatant was then centrifuged for 10 min at 9000 ×*g* and the resulting pellet was suspended in isolation medium without BSA and centrifuged for 10 min at 10,000 ×*g*. The final mitochondrial pellet was suspended in isolation medium without BSA, to a final protein concentration of approximately 40 mg/mL. All procedures were carried out on ice and the centrifugation steps were performed at 4 °C. Experiments were performed using mitochondrial preparations with high respiratory control ratios (RCRs of 8–9) indicating that the isolated mitochondria are of high functional quality with a high capacity for oxidation of respiratory substrates, effective ATP synthesis and a low degree of proton leak [35,36].

2.5. High-resolution respirometry

Respiration in intact cells, freshly isolated mitochondria and freeze-thawed mitochondrial preparations was monitored with high-resolution respirometry (OROBOROS Oxygraph-2 k, Innsbruck, Austria) using a chamber volume set to 2 mL [37]. Calibration with air-saturated medium was performed daily. Data acquisition and analysis were carried out using Datlab software (OROBOROS Instruments).

2.5.1. Intact H1299 cells

H1299 cells were suspended (in growth medium) in the 2 mL glass chamber at a density of 2.5×10^5 cells/mL at 37 °C and thereafter investigated using a phosphorylation control protocol [38] (Supplementary Fig. S1). Cellular respiration was first allowed to stabilize at steady-state without any additions to the cell medium. At steady-state respiration (O_2 consumption), the respiratory flux is constant. This defines the ROUTINE respiration state (i.e. the physiological coupling state controlled by cellular energy demands). After observing ROUTINE state for 10 min, PEI or H_2O (control) was added to the chamber. After incubation with PEI (at 5, 30 or 60 min), the ATP synthase was inhibited by addition of oligomycin (2 μg/mL) in order to detect the level of LEAK respiration. The LEAK state of respiration is independent of ADP phosphorylation, and mainly occurs due to proton leak from the mitochondrial intermembrane space [38–40]. The maximal capacity of the ETS was obtained by stepwise titrations (0.5 μM) with the protonophore, carbonyl cyanide m-chlorophenylhydrazone (CCCP) until maximal respiratory flux could be detected [38]. Following this, respiration was sequentially inhibited by addition of rotenone (Rote) at 0.5 μM, to selectively inhibit CI, and then antimycin A (Anti-A) at 2.5 μM, to inhibit the activity of CIII. The resulting state provides a measure of residual oxygen consumption (ROX). Mitochondrial respiration was corrected for oxygen flux due to instrumental background and ROX [37–39]. The rate of mitochondrial ATP synthesis (oligomycin-sensitive respiration) was calculated as the difference between ROUTINE respiration and LEAK respiration.

2.5.2. Freshly isolated mouse liver mitochondria

Respiration in isolated mitochondria was investigated at 25 °C in a mitochondrial respiration medium (MIR05) containing EGTA 0.5 mM, $MgCl_2$ 3 mM, K-lactobionate 60 mM, Taurine 20 mM, KH_2PO_4 10 mM, HEPES 20 mM, sucrose 110 mM and BSA free from fatty acids 1 g/L, pH 7.1 [38]. Respiring mitochondria were supplemented with respiratory substrates (glutamate 5 mM, malate 5 mM and succinate 10 mM) for combined electron flow through CI and CII [39]. In all experiments, the following protocol was applied (Supplementary Fig. S2), using a mitochondrial protein content of 0.2–0.3 mg/mL. Briefly, leak mitochondrial respiration (state 2) was first allowed to stabilize in the presence of respiratory substrates without the addition of ADP to the respiration medium. Next, 25k-PEI-B or H_2O (control) was added to the mitochondrial suspension and incubated

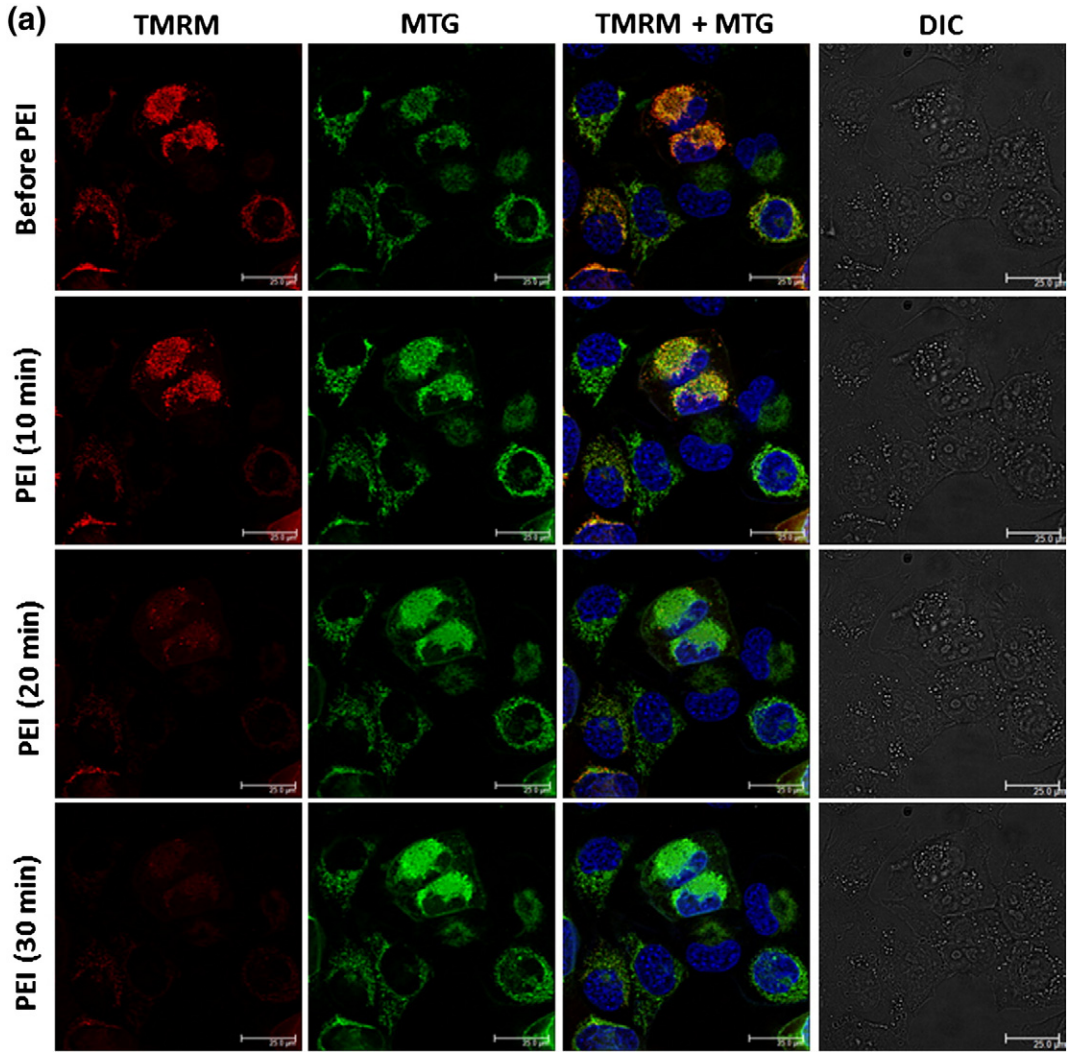

Fig. 1. The relationship between mitochondrial membrane potential ($\Delta\psi_m$) and cell death following PEI challenge in H1299 cells. Cells were loaded with MTG, TMRM and the nuclear dye Hoechst-33342 in growth medium for 20 min at 37 °C. After staining, cells were washed twice and challenged with 25k-PEI-B (10 μg/mL) in growth medium at 37 °C followed by live cell imaging at different time intervals, panel (a). MTG accumulates in the mitochondria independent of the $\Delta\psi_m$, whereas TMRM accumulates in a $\Delta\psi_m$-dependent manner. Since cationic TMRM and MTG were both initially taken up only by polarized mitochondria, the gradual loss of TMRM red fluorescence and recovery of the green fluorescence of covalently bound MTG indicate loss of $\Delta\psi_m$ on PEI challenge. This is also confirmed in the loss of yellow in the overlay images. Scale bar = 25 μm. Panel (b) shows quantification of TMRM and MTG fluorescence intensity by FACS, whereas the scatterplots in panel (c) represent changes in cellular size (FS) and granularity (SS) following PEI exposure. Panel (d) is representative of PEI-mediated cell death events monitored by propidium iodide (PI) staining. PI nuclear staining becomes prominent from 60 min and onward. Scale bar = 20 μm.

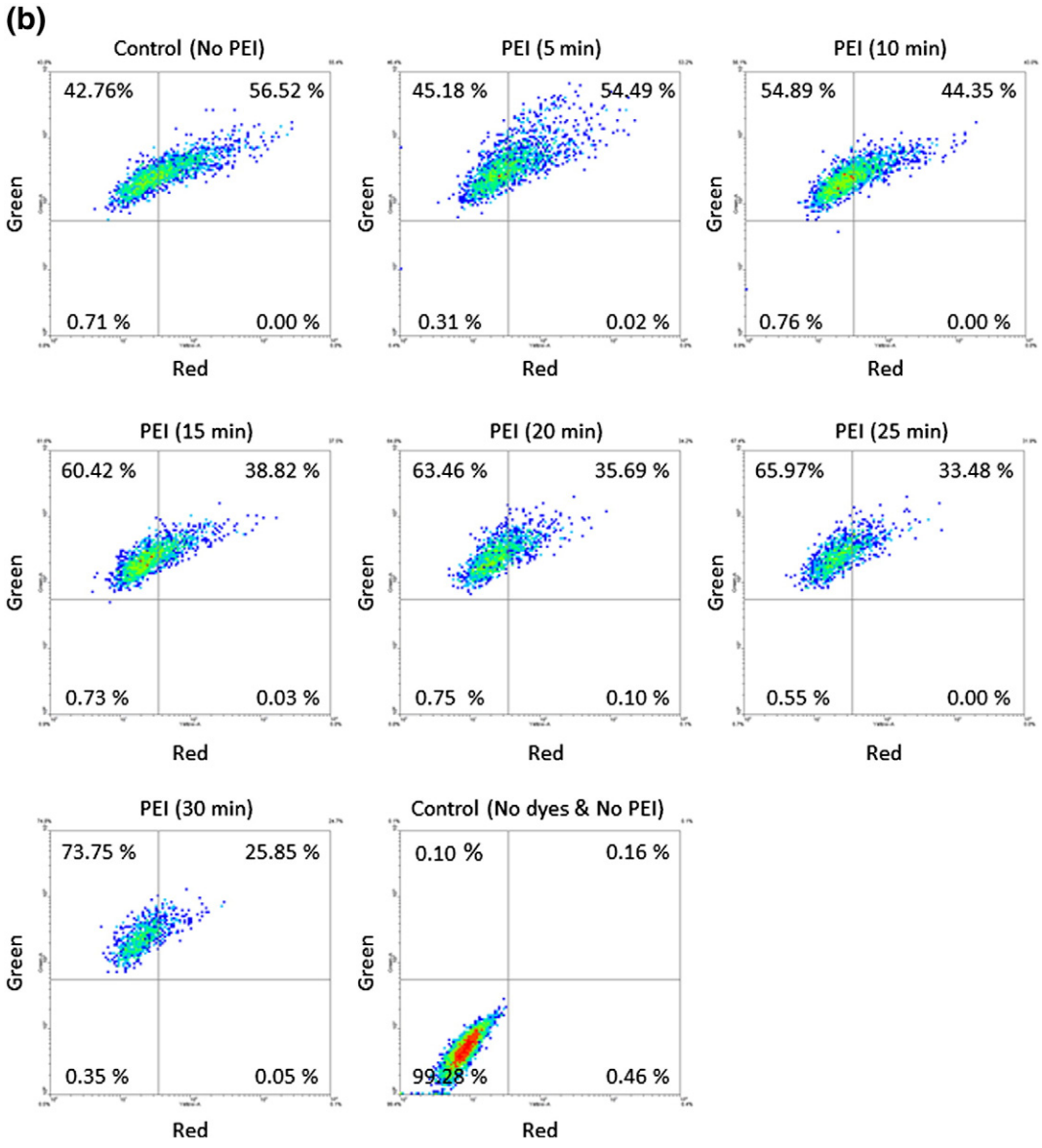

Fig. 1 (*continued*).

for 15 or 30 min, followed by addition of ADP at saturating concentration (2.5 mM). This results in maximal, ADP-stimulated respiration (state 3) and ATP synthesis by the mitochondrial F_0/F_1-ATP synthase [39,41]. Subsequent addition of oligomycin (2 μg/mL) was added to achieve non-phosphorylating leak respiration (state 4o), mainly driven by proton leak from the mitochondrial intermembrane space after oligomycin-mediated inhibition of the ATP synthase [39,40]. Finally, respiration was selectively inhibited first by addition of rotenone at 0.5 μM and next Anti-A at 2.5 μM, to inhibit CI and CIII, respectively, providing measure of ROX. Mitochondrial respiration was corrected for oxygen flux due to instrumental background and ROX [38,39]. Mitochondrial ATP synthesis was calculated as the difference between state 3 and state 4o.

2.5.3. 'Broken mitochondrial' preparation

The interference of 25k-PEI-B with components of the ETS was investigated in a 'broken mitochondrial' preparation (0.3–0.4 mg/mL final protein concentration) at 25 °C in MIR05. 'Broken mitochondria' were obtained by three freezing–thawing cycle disruption of isolated mouse liver mitochondria suspended in isolation medium (mannitol 225 mM, sucrose 75 mM, Tris–HCl 5 mM, EGTA 0.1 mM, at pH 7.0). A combination of succinate (10 mM) and NADH (1 mM) was used to divert electrons simultaneously through CI and CII, together with external addition of cyt *c* (10 μM) to obtain steady flow of electrons from CIII to CIV [38,39]. Additions of 25k-PEI-B (1 μg/mL per step) were applied to investigate the potential interference of PEI with the protein complexes of the electron transport system. At the end of each experiment, 0.5 mM potassium cyanide (KCN) was added to obtain a measure of ROX. Oxygen consumption by the ETS was corrected for oxygen flux due to instrumental background and ROX [38,39]. In addition, the effect of PEI on electron flow through CI–CIII–CIV was investigated in 'broken mitochondria' in the presence of NADH (1 mM) to divert electrons through CI, together with external addition of cyt *c* (10 μM) in order to obtain a steady flow of electrons from CIII to CIV [38,39]. Furthermore, the effect of PEI on electron flow through CII–CIII–CIV was investigated in the presence of succinate (10 mM) to divert electrons through CII, together with rotenone (2.5 μM) to inhibit CI and external addition of cyt *c* (10 μM) to obtain steady flow of electrons from CIII to CIV [38,39]. Finally, the activity of CIV was investigated in the presence of 0.5 mM *N*,*N*,*N*′,*N*′-tetramethyl-*p*-phenylenediamine (TMPD), 2 mM ascorbate (Asc), 10 μM cyt *c*, 2.5 μM rotenone, 5 mM malonic acid (Mna) and 2.5 μM Anti-A following sequential additions of different

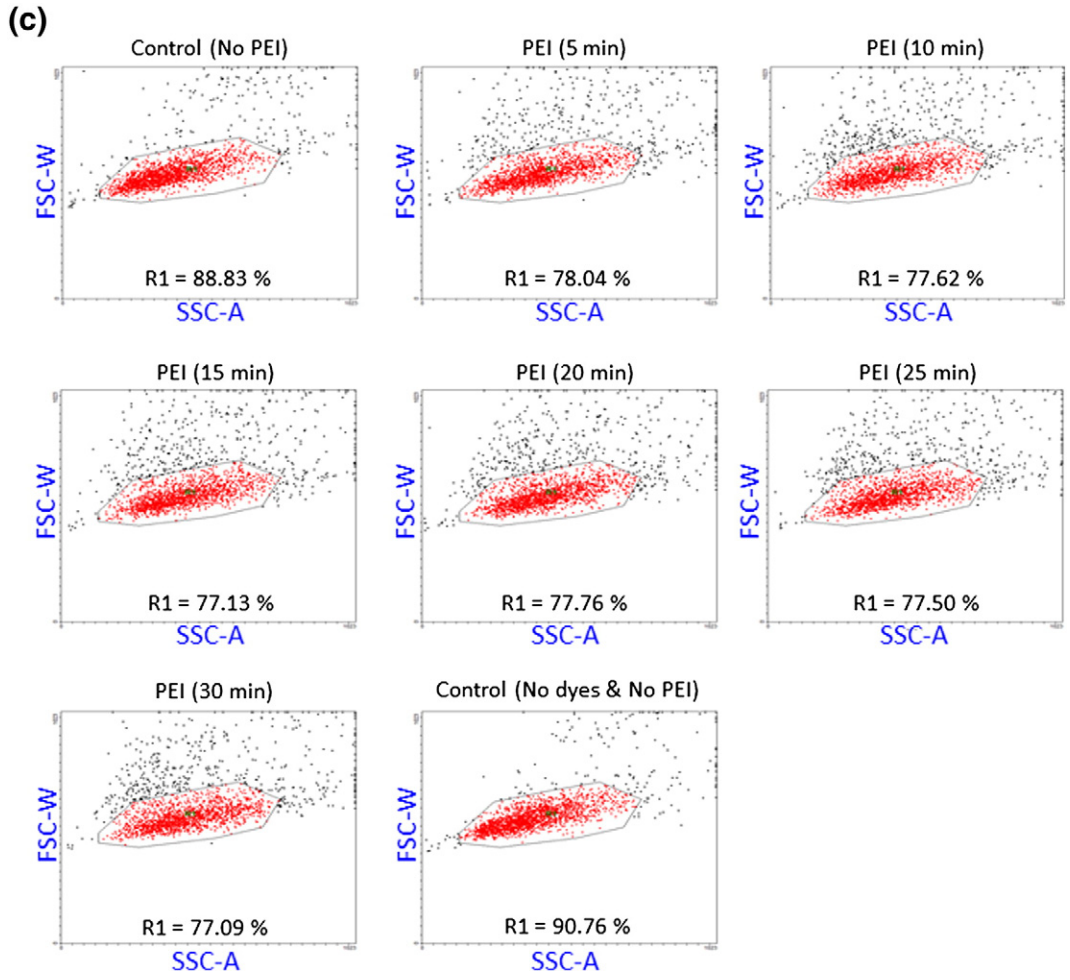

Fig. 1 (*continued*).

concentrations of 25k-PEI-B. Finally, 100 mM sodium azide (NaN_3) was added to inhibit CIV activity, providing measure of ROX. Oxygen consumption by the ETS was corrected for oxygen flux due to instrumental background and ROX [38,39].

2.6. Spectrophotometric analysis of CIV activity

The activity of CIV was investigated in a 'broken mitochondrial' preparation (4.8 μg final protein concentration per sample) in the presence of different concentrations of 25k-PEI-B using cyt *c* oxidase assay kit (Sigma-Aldrich). Briefly, the CIV activity was monitored at $\lambda = 550$ nm in a Tecan microplate reader (Infinite M200, Tecan Nordic AB, Sweden) and following absorbance measurements, calculations of CIV activity (nmol/min/mg) were performed according to manufacturer's instructions.

2.7. ATP determination

The concentration of ATP was determined using a modified method based on the ATPlite luminescence assay system (Perkin-Elmer). Briefly, H1299 cell suspensions (2.5×10^5 cells/mL) were incubated with 25k-PEI-B for appropriate times at 37 °C in growth medium. In parallel, experiments were done using high-resolution respirometry. Following incubation, the cell pellet was separated from the medium by centrifugation at 500 ×*g* for 5 min at 4 °C in order to obtain separate measurements of intra- and extracellular ATP. After separation the samples were left on ice to slow down degradation of the ATP molecules and the samples were quickly mixed with lysis solution (2:1 medium:cell lysis buffer) (ATPlite, Perkin Elmer). ATP concentrations were measured based on triplicate aliquots taken from the sample in 3:1 ratio with substrate solution (ATPlite, Perkin Elmer). Luminescence was recorded in a Tecan microplate reader (Infinite M200, Tecan Nordic AB, Sweden).

2.8. Trypan blue exclusion test

Trypan blue staining was used to investigate the effects of PEI exposure on plasma membrane damage. Briefly, suspensions of 2.5×10^5 cells/mL were incubated with 25k-PEI-B at 37 °C in growth medium for appropriate times. Following PEI exposure, cells were stained with trypan blue and counted under the microscope. Data is presented as % of cells excluding trypan blue.

2.9. Statistical analysis

Results are expressed as means ± SD from at least three independent experiments except stated otherwise. Statistical analyses and comparison of different groups in relation to one or two factors were performed with one-way ANOVA or two-way ANOVA as appropriate. The Bonferroni method was subsequently used to correct *p* values after multiple comparisons to calculate statistical significance.

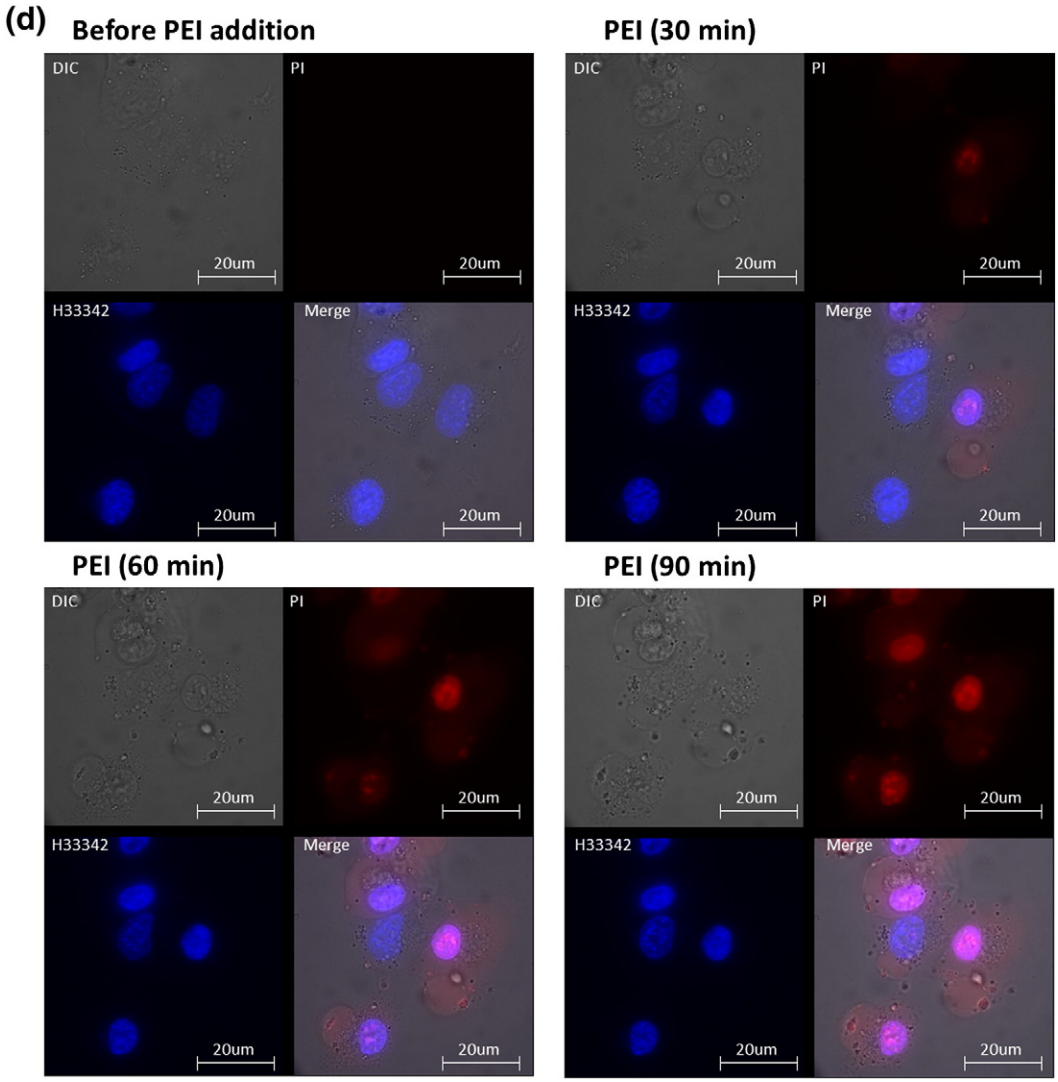

Fig. 1 (*continued*).

Values of $p < 0.05$ post Bonferroni corrections were taken as the level of significance.

3. Results

3.1. Loss of $\Delta\psi_m$ precedes cell death in H1299 cells on PEI exposure

The loss of $\Delta\psi_m$ plays a key role in mitochondrial-mediated cell death [19]. Accordingly, we followed the effect of PEI on $\Delta\psi_m$ in H1299 cells co-loaded with MTG and TMRM. PEI (10 μg/mL) induced gradual time-dependent loss of $\Delta\psi_m$ starting within 10 min of exposure (Fig. 1a, b). However, the FS/SS scatterplots, where FS reflects cell size and SS cell granularity, indicated that by 30 min of PEI exposure the majority of cells (represented in a contour of equal probability density in the distribution of untreated cells) are in viable state (Fig. 1c). Observations with H1299 cells stained with PI and Hoechst-33342 (Fig. 1d) further corroborate with these findings. Cell death, however, becomes prominent at longer exposure time (90 min). Collectively, these results show that H1299 cells are highly sensitive to PEI exposure and may serve as a convenient model to investigate the likely mechanism(s) by which PEI could induce mitochondrial failure at early time points (under 30 min), where the majority of cells are still in viable state.

3.2. PEI-mediated changes on mitochondrial respiratory states in intact cells

The results in Fig. 2 show how PEI at different concentrations severely affects various respiratory states in H1299 cells, based on a standardized phosphorylation control titration protocol (Supplementary Figs. S1, S3 and S4). PEI affected ROUTINE respiration in a concentration and time-dependent manner (Fig. 2a). Within 5 min of addition, PEI significantly increased O_2 flux at concentrations above 5 μg/mL. This initial PEI concentration-dependent respiratory increase, however, was followed by a gradual decline over time. The effect was more prominent with a PEI concentration of 10 μg/mL (starting at 30 min), but with lower concentrations (5 μg/mL) the respiratory decline (O_2 flux) became significantly different at later time points (60 min).

In parallel with ROUTINE respiration, PEI also increased LEAK respiration in a concentration-dependent manner at 5 min of exposure (Fig. 2b). By 30 min, the PEI-mediated increase in LEAK respiration declined and the values were comparable with the control incubation. Only at 60 min the decline was significantly lower with a PEI concentration of 10 μg/mL (Fig. 2b). The decline phase became more prominent with higher PEI concentrations and observable within 30 min of exposure (data not shown). PEI was also found to significantly inhibit the maximal capacity of the ETS, again in a concentration- and time-dependent manner (Fig. 2c). Here, PEI at 3 μg/mL was capable

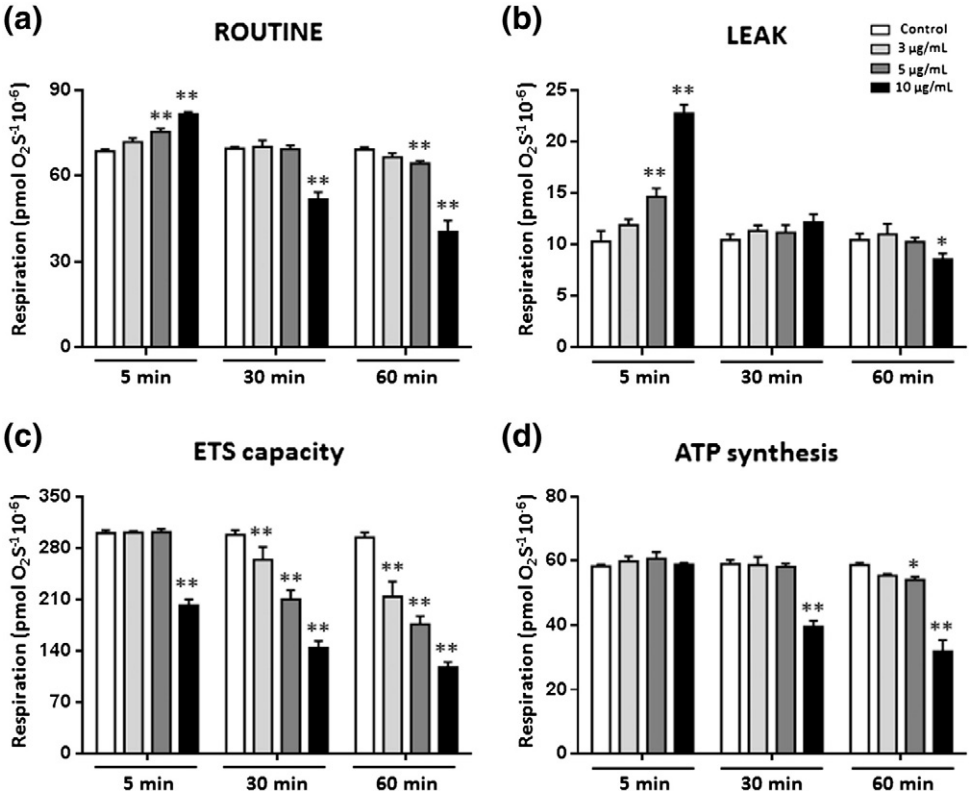

Fig. 2. The effect of PEI concentration on respiratory states and ATP synthesis in H1299 cells. Respiration (indicated as the rate of oxygen consumption or O_2 flux) was evaluated at different stages (ROUTINE, LEAK, ETS and ATP synthesis) on PEI challenge (3–10 μg/mL). Statistical analyses were performed with two-way ANOVA, using Bonferroni multiple comparison correction to calculate significance ($^*p < 0.05$, $^{**}p < 0.01$).

of significantly reducing ETS after 30 min of incubation. Furthermore, the results in Fig. 2d show that PEI affects mitochondrial ATP synthesis (oligomycin-sensitive respiration). The reduced capacity of intact mitochondria to synthesize ATP is significantly observed with PEI levels of 5 μg/mL at longer periods of time (60 min) as well as with higher concentrations but at shorter periods of incubation (30 min).

Next, we calculated the effect of PEI concentration and exposure time on corresponding respiratory flux ratios (RFRs) (Table 1). The RFRs are defined as O_2 flux in different respiratory control states, normalized for maximum flux of the ETS capacity, acquiring theoretically lower and upper limits of 0.0 and 1.0 [38,39]. PEI increased RFR values in a time- and concentration-dependent manner. However, at 10 μg/mL PEI-augmented RFR values declined on longer exposure time when compared with controlled cells. The ROUTINE control ratio (R/E) is the ratio of ROUTINE (R) respiration and ETS (E) capacity; this gives an estimate of how close ROUTINE respiration operates to the ETS capacity. An increasing R/E is indicative of increasing cellular ATP demand, mitochondrial uncoupling and/or the limitation of respiratory capacity by impaired activity of ETS components [38]. The LEAK control ratio (L/E) is the ratio of LEAK (L) respiration and ETS capacity. When the ETS capacity remains constant, L/E provides an estimation of mitochondrial uncoupling. Pathological uncoupling can be caused by toxic external agents and is thus distinct from intrinsic uncoupling [38]. The data summarized in Table 1 indicates that the early concentration-dependent increases in L/E ratios are a result of PEI mediated uncoupling of the mitochondria as LEAK respiration is significantly increased following 5 min incubation with 5 μg/mL PEI (Fig. 2b), whereas the ETS capacity remains constant (Fig. 2c). The netROUTINE control ratio ((R-L)/E) represents the phosphorylation related respiration as a fraction of ETS capacity. This provides an estimation of cell functioning with respect to its bioenergetic limit [38]. The early (5 min) increase in LEAK respiration at lower PEI concentrations (3 and 5 μg/mL) (Fig. 2b) is fully compensated by increased ROUTINE respiration (Fig. 2a). Consequently, the (R-L)/E is unaffected and mitochondrial ATP synthesis is maintained at a constant rate (Fig. 2d). At later time points (30 and 60 min), the changes in (R-L)/E result

Table 1
Flux ratios in intact cells following incubation with 25k-PEI-B.

25k-PEI-B	RCR "R/E"			LCR "L/E"			netRCR "(R-L)/E"		
Time [min]	5	30	60	5	30	60	5	30	60
Control	0.229 ± 0.010	0,233 ± 0.006	0.235 ± 0.008	0.034 ± 0.004	0.035 ± 0.002	0.036 ± 0.003	0.194 ± 0.004	0.198 ± 0.007	0.199 ± 0.005
3 μg/mL	0.238 ± 0.002	0.266 ± 0.014*	0.313 ± 0.036**	0.042 ± 0.001	0.039 ± 0.004	0.052 ± 0.010**	0.197 ± 0.002	0.227 ± 0.014	0.262 ± 0.026**
5 μg/mL	0.250 ± 0.002	0.331 ± 0.022**	0.367 ± 0.025**	0.049 ± 0.003**	0.053 ± 0.003**	0.058 ± 0.006**	0.202 ± 0.004	0.278 ± 0.020**	0.307 ± 0.019**
10 μg/mL	0.404 ± 0.020**	0.362 ± 0.013**	0.303 ± 0.007**	0.113 ± 0.009**	0.075 ± 0.007**	0.066 ± 0.012**	0.292 ± 0.011**	0.286 ± 0.017**	0.238 ± 0.017**

Flux ratios are calculated as the means ± SD for 3 parallel experiments. Statistical analyses were performed with two-way ANOVA, using Bonferroni multiple comparison correction to calculate significance ($^*p < 0.05$; $^{**}p < 0.01$). The ROUTINE control ratio (R/E) is the ratio of ROUTINE (R) respiration and ETS (E) capacity. The R/E gives an estimate of how close ROUTINE respiration operates to the ETS capacity. The LEAK control ratio (L/E) is the ratio of LEAK (L) respiration and ETS capacity. The L/E provides an estimation of mitochondrial uncoupling when the ETS capacity remains constant. The netROUTINE control ratio ((R-L)/E) represents phosphorylation related respiration as a fraction of ETS capacity. After 5 min exposure with 3 and 5 μg/mL PEI the increase in LEAK respiration (Fig. 2b) is fully compensated by increasing ROUTINE respiration (Fig. 2a) and therefore no changes are observed in the (R-L)/E.

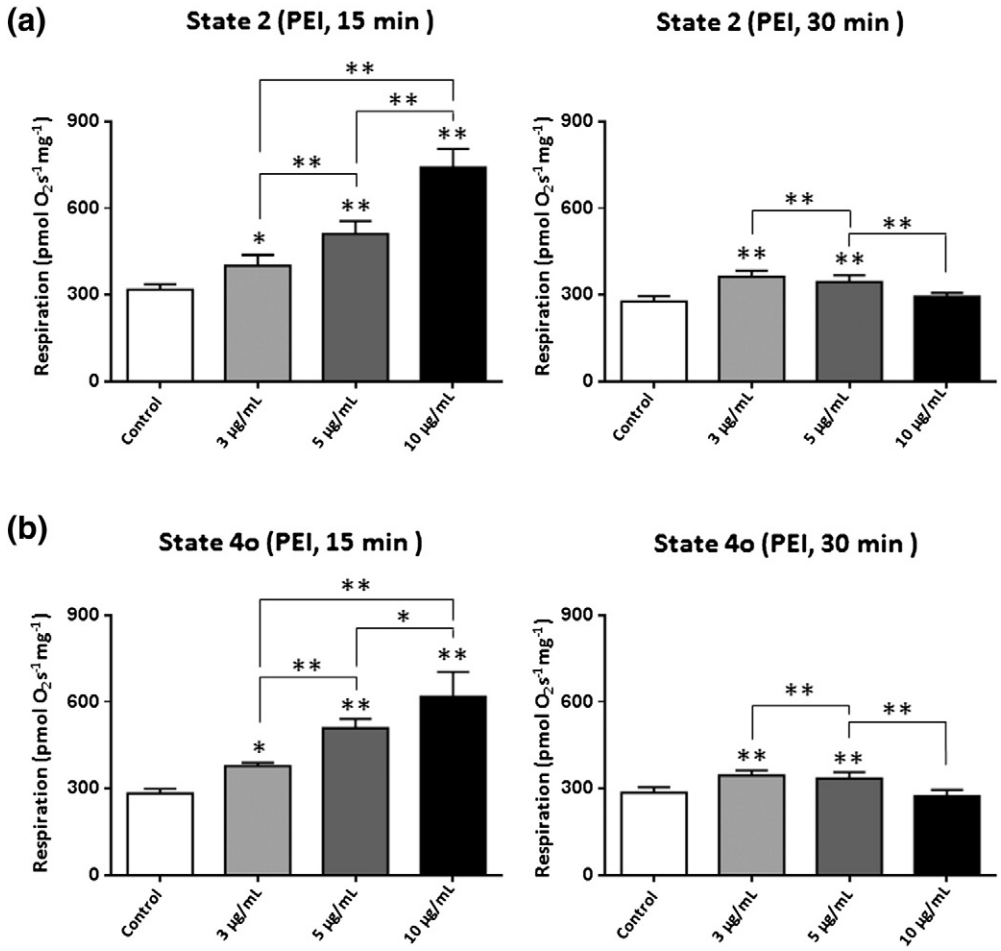

Fig. 3. The effect of PEI concentration on mitochondrial proton leak in isolated mouse liver mitochondria. Panels (a) and (b) show the effect of PEI concentration on state 2 and 4o respirations, respectively at two different time points. Bars represent the mean ± SD of 5 parallel experiments. Statistical analyses (with respect to control and between indicated pairs) were performed with repeated measurement one-way ANOVA, using Bonferroni multiple comparison correction to calculate significance (*$p < 0.05$, **$p < 0.01$).

from gradual decline of the ETS capacity following PEI exposure (Fig. 2c) thus driving cells to utilize more of their respiratory capacity to maintain constant ATP synthesis.

3.3. PEI-mediated changes on respiratory states in freshly isolated mouse liver mitochondria

The results in Fig. 3 show the effect of different PEI concentration on the respiratory functions of well-coupled, freshly isolated mouse liver mitochondria at two different time points. PEI exposure for 15 min significantly increased both state 2 and state 4o O_2 fluxes (Fig. 3a & b). Increased O_2 flux during state 4o respiration is indicative of accelerated proton leak or proton transfer across the inner mitochondrial membrane [35,38,39]. The increased proton leak, however, declined after longer incubation periods (30 min) with higher PEI levels (5 and 10 μg/mL). Furthermore, PEI significantly lowered the ability of the mitochondria to phosphorylate ADP (state 3) in a time- and concentration-dependent manner (Fig. 4a). Notably, the lowest PEI-concentration tested (3 μg/mL) increased proton leak significantly after 15 min (Fig. 3a & b), although state 3 respiration was not declined until after 30 min incubation (Fig. 4a). Correlating with the observed PEI-mediated effect on state 3 and state 4o respiration, mitochondrial ATP synthesis (oligomycin-sensitive respiration) also significantly decreased at all tested PEI concentrations (Fig. 4b; representative oxygraph traces are shown in Supplementary Figs. S5–S7).

The results in Table 2 summarize the calculated mitochondrial respiratory control ratios (RCRs) as indicators of PEI-induced mitochondrial dysfunction. High RCR values imply high mitochondrial capacity for oxidation of respiratory substrates, ATP synthesis and a low degree of proton leak [35]. The results clearly show that RCR values decrease significantly in response to the increasing concentrations of the polycation (Table 2).

3.4. PEI acts as a potent inhibitor of ETS activity in 'broken mitochondria'

We next examined the consequence of exposing ETS components directly to PEI. Therefore, the activity of the ETS (O_2 flux) was monitored using a 'broken mitochondrial' preparation following the addition of PEI in the presence of combined electron flow into the ETS through CI and CII [39].

These results strongly suggest that PEI is a potent inhibitor of the ETS even at 1 μg/mL (Supplementary Fig. S8). To pinpoint the specific site of PEI mediated inhibition within the ETS, we used a substrate combination to feed electrons specifically to either CI or CII. The results in Fig. 5a–d show that PEI both impairs electron transport through CI–CIII–CIV and CII–CIII–CIV, suggesting that PEI is acting as an inhibitor of electron flow downstream of both CI and CII. Notably, the CIV catalyzes transfer of electrons from cyt *c* to oxygen through electrostatic interactions [42] and due to its polycationic nature PEI could perhaps interfere with these processes. By using both high-resolution respirometry and spectrophotometric-based cyt *c* oxidase activity measurements, we found that even at very low concentrations (0.1–0.5 μg/mL) PEI acts as a potent inhibitor of CIV activity (Figs. 5e–f & 6).

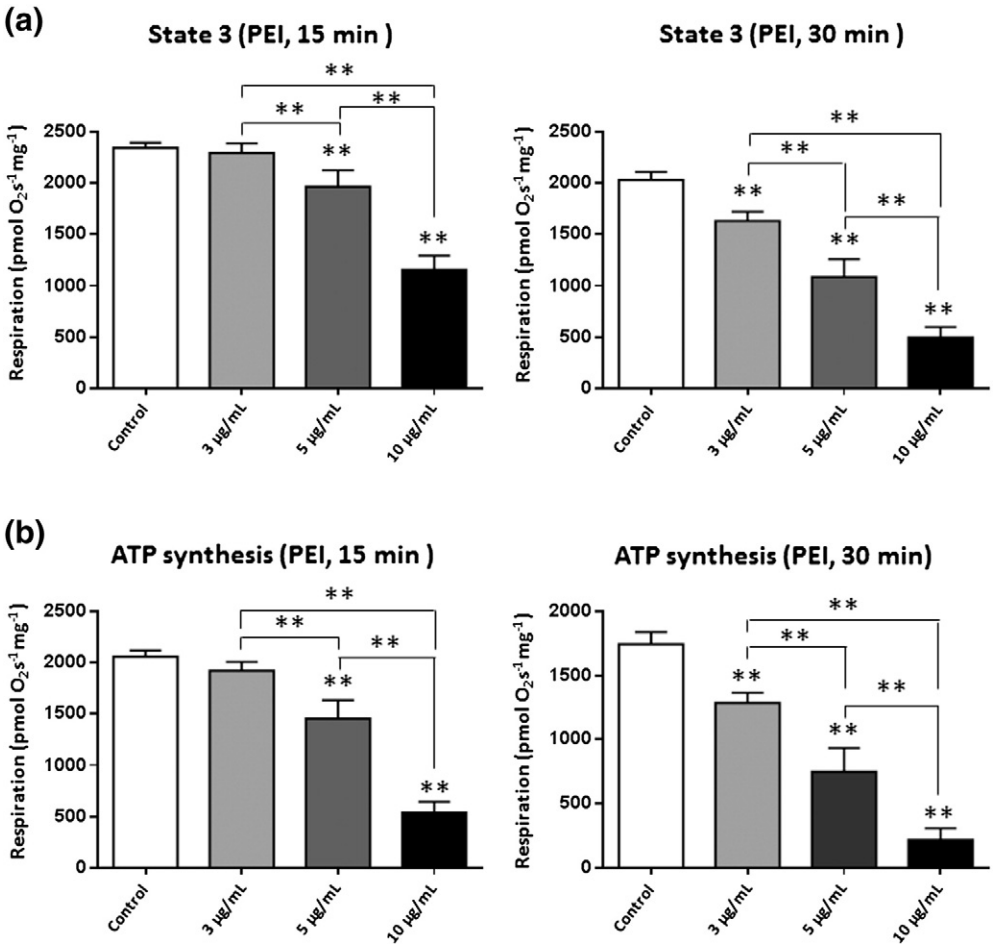

Fig. 4. The concentration-dependent effect of PEI on mitochondrial state 3 respiration and ATP synthesis (oligomycin-sensitive respiration) in isolated mouse liver mitochondria. Bars represent the mean ± SD of 5 parallel experiments. Statistical analyses (with respect to control and between indicated pairs) were performed with repeated measurement one-way ANOVA, using Bonferroni multiple comparison correction to calculate significance (*$p < 0.05$, **$p < 0.01$).

3.5. The effect of PEI on intracellular ATP levels and plasma membrane integrity

Addition of PEI to H1299 cells dramatically reduced the levels of intracellular ATP in a concentration-dependent manner (Fig. 7a). This is fully in line with the abovementioned observations on PEI-mediated proton leak, impaired ETS capacity and decreased ATP synthesis. However, the extent of ATP loss remains similar at different time points for each particular PEI concentration. In parallel, the extracellular ATP levels increased on increasing PEI concentration (Fig. 7b), but the accumulated ATP levels did not fully account for the total loss of intracellular ATP. This presumably indicates reduced mitochondrial ATP synthesis (or increased cellular ATP consumption), which is in line with the results in Figs. 2 & 4. The data in Fig. 7c further show that PEI dramatically reduces plasma membrane integrity even at low concentrations (3 μg/mL); this may account for the appearance of extracellular ATP.

Table 2
Mitochondrial respiratory control ratio (RCR) (state 3/state 4o).

25k-PEI-B	Control	3 μg/mL	5 μg/mL	10 μg/mL
[15 min]	8.3 ± 0.173	6.5 ± 0.503**	4.9 ± 0.789**	2.1 ± 0.251**
[30 min]	8.1 ± 0.255	5.9 ± 0.301**	3.8 ± 0.439**	2.0 ± 0.311**

RCR is calculated as mean ± SD for 5 parallel experiments. Statistical analyses were performed with two-way ANOVA and Bonferroni multiple comparison correction to calculate significance (**$p < 0.01$).

4. Discussion

To the best of our knowledge, this is the first study demonstrating concentration- and time-dependent effect of PEI on mitochondrial proton leak and its inhibitory effect on the ETS in intact cells. Indeed, we have now demonstrated that extracellular PEI at a concentration range of 3–5 μg/mL can rapidly (within 5 min) induce mild mitochondrial uncoupling in H1299 cells. This is shown by the fact that the increase in L/E ratio (Table 1) occurs only due to increased proton leak as a result of increased LEAK respiration, whereas the ETS capacity remains unchanged (indicative of PEI-mediated proton leak). Interestingly, subsequent to PEI-induced increase in mitochondrial proton leak, PEI also caused a concentration-dependent decline in proton leak at later time points. This suggests that PEI exerts additional effects on mitochondrial functions. Moreover, PEI further induced significant concentration- and time-dependent inhibitory effect on the ETS capacity in intact cells, which presumably is due to impairment of substrate oxidation [38]. It should be emphasized that although mitochondrial permeabilization could lead to reduced OXPHOS capacity, mitochondrial permeabilization alone is not capable of inhibiting electron transfer and substrate oxidation by the ETS components [20,21,43–45]. However, reduction of state 3 respiration in isolated mitochondria could be induced by impaired substrate oxidation [35]. Therefore, we speculate that PEI has an inhibitory role on the ETS components. Earlier attempts with other types of polycations (e.g., polylysines) demonstrated their inhibitory effect on CIV activity [46]. In line with these suggestions, experiments with 'broken mitochondrial' preparations

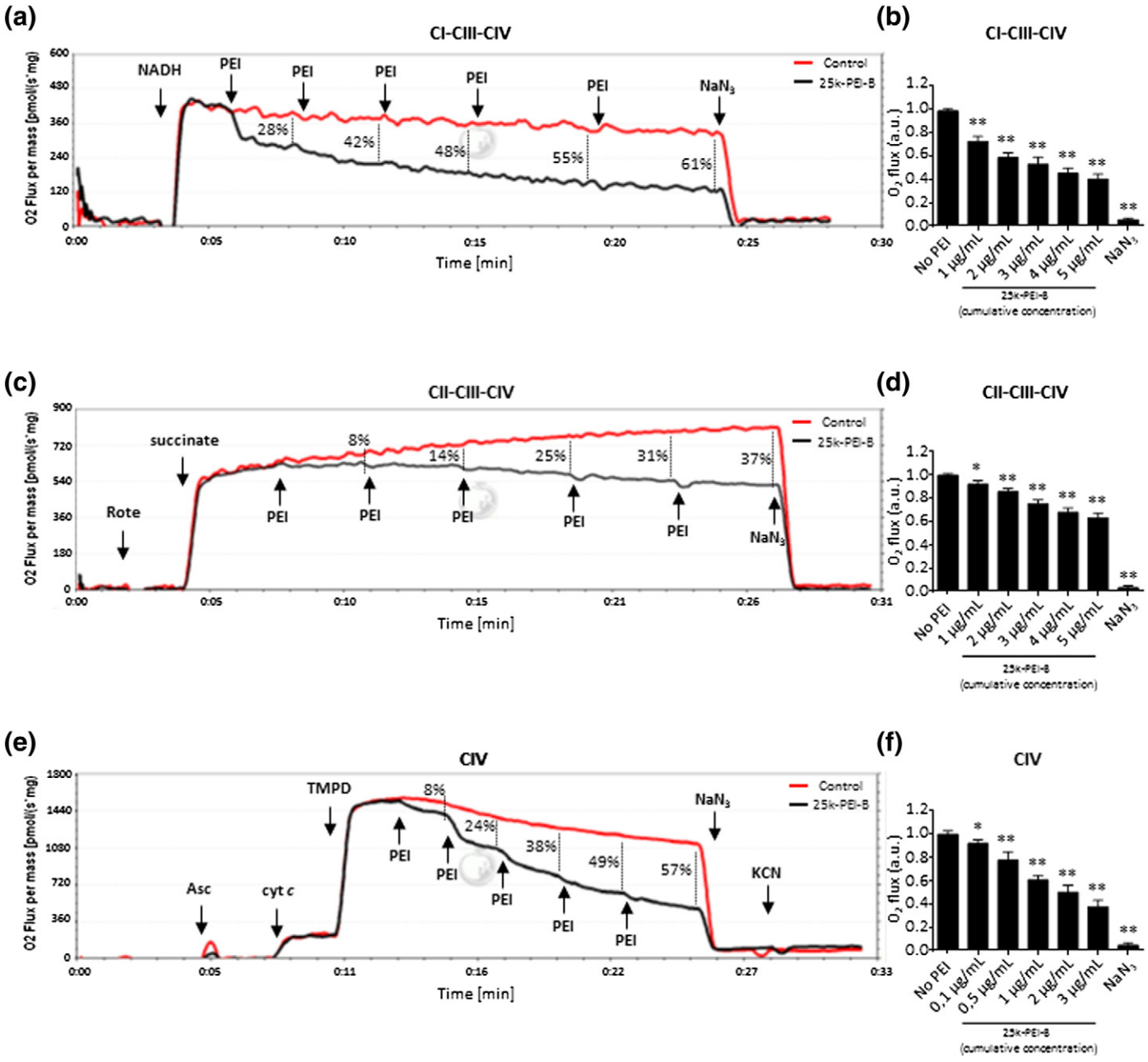

Fig. 5. The inhibitory effect of PEI on the electron transport system activity in 'broken mitochondria'. Oxygen consumption (O_2 flux) was measured in a substrate combination of NADH and cyt *c* or combination of succinate, rotenone (Rote) and cyt *c* for specific electron flux through CI–CIII–CIV or CII–CIII–CIV, respectively. Moreover, the activity of CIV was measured with combination of TMPD, ascorbate (Asc), cyt *c*, rotenone, antimycin-A and malonic acid. Panels (a) and (c) represent high resolution respirometry and representative trace of oxygen flux through CI–CIII–CIV and CII–CIII–CIV in 'broken mitochondria', respectively. Oxygen consumption was measured on five cumulative additions of 25k-PEI-B (1 μg/mL per addition). Panels (b) and (d) show reduction of CI–CIII–CIV and CII–CIII–CIV activity in 'broken mitochondria' exposed to cumulative concentrations of PEI relative to control, respectively. Bars represent the mean ± SD of 4 parallel experiments. Panel (e) shows high-resolution respirometry and representative trace of oxygen flux through CIV in 'broken mitochondria'. Oxygen consumption was measured on five cumulative additions of 25k-PEI-B (first addition: 0.1 μg/mL, second addition: 0.4 μg/mL, third addition: 0.5 μg/mL, fourth and fifth additions: 1 μg/mL each). Panel (f) shows relative reduction of CIV activity in 'broken mitochondria' following exposure to different concentrations of PEI. Bars represent the mean ± SD of 4 parallel experiments. Statistical analyses were performed with one-way ANOVA, using Bonferroni multiple comparison correction to calculate significance ($^*p < 0.05$, $^{**}p < 0.01$).

confirmed that PEI inhibits electron flow and substrate oxidation by the ETS due to its potent inhibitory effect at least on CIV activity even at very low concentrations. The observation that PEI inhibits ETS activity correlates well with the fact that the early increase of mitochondrial proton leak following PEI exposure declines again at later time points. Consequently, ETS translocates fewer protons over the inner membrane and therefore fewer protons are available in the intermembrane space to leak back through the inner membrane into the matrix, explaining partially why the early acceleration of mitochondrial proton leak following PEI exposure declines with longer incubation times. Collectively, the experimental evidence shows that in addition to induce mitochondrial proton leak, PEI acts as a potent inhibitor of the ETS by inhibiting the activity of CIV.

PEI-mediated mitochondrial destabilization is conceivably a consequence of the membrane perturbation properties of the polycation and formation of nanoscale pores in a similar manner to the function of pore-forming peptides [3]. These processes are presumably similar to the function of pore-forming peptides such as alamethicin, which also possesses high affinity toward mitochondrial membranes as their membrane insertion and pore forming ability are largely driven by the

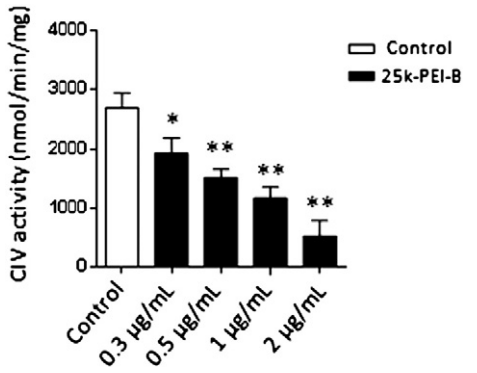

Fig. 6. Determination of the inhibitory effect of PEI on CIV activity in 'broken mitochondria' by spectrophotometric analysis of cytochrome *c* oxidase activity. Bars represent the mean ± SD of 3 parallel experiments. Statistical analyses were performed with one-way ANOVA, using Bonferroni multiple comparison correction to calculate significance ($^{*}p < 0.05$, $^{**}p < 0.01$).

$\Delta\psi_m$ [47]. These pore-forming peptides induce nonspecific permeability changes, which can result in swelling and disruption of the mitochondria [48]. Similarly, 25k-PEI-B was recently shown to induce swelling of isolated rat liver mitochondria at low concentrations [30]. On the basis of these speculations, the cytoplasmic concentration of functional PEI must be sufficiently enough to induce the observed mitochondrial perturbations. PEI enters cytoplasm most likely through plasma membrane, as a result of electrostatic interactions and its detergent activity [3], and endosome destabilization (most likely arising from PEI-mediated membrane fragment micellization) [3,49]. Recent studies also attest that fluorescently labeled extracellular PEI reaches mitochondria in intact cells [17].

Mitochondrial ATP synthesis is dependent on the electrochemical proton gradient [20,21]. Correspondingly, we observed significant reduction in mitochondrial ATP synthesis and drop in intracellular ATP levels after PEI exposure, which may partly arise due to increased ATP consumption. We also found that the intracellular ATP depletion was partly a consequence of PEI induced damage to the plasma membrane and ATP leakage. Previous studies have shown that PEI can induce cell death through both apoptotic and necrotic pathways [4,10]. It has also been suggested that mild reductions in intracellular ATP levels could trigger apoptosis, whereas profound ATP depletion may initiate necrosis [27,28,50]. It is therefore conceivable that PEI-induced necrotic and/or apoptotic cell death processes are driven by the magnitude of bioenergetic crisis (mitochondrial uncoupling, impaired ETS activity and diminished ATP synthesis) and the extent of plasma membrane destabilization, which in turn depends on the initial PEI concentration. Accordingly, PEI could induce apoptosis in a stochastic manner, with different cells entering apoptosis at different times depending on the extent of plasma membrane damage, intracellular PEI levels and its effect on mitochondrial ATP synthesis. With profound plasma membrane damage ATP leakage is accelerated, which together with diminished ATP synthesis may trigger cell death predominantly through necrosis. The 25k-PEI-B also accumulates in lysosomes without inducing change in lysosomal pH [49].

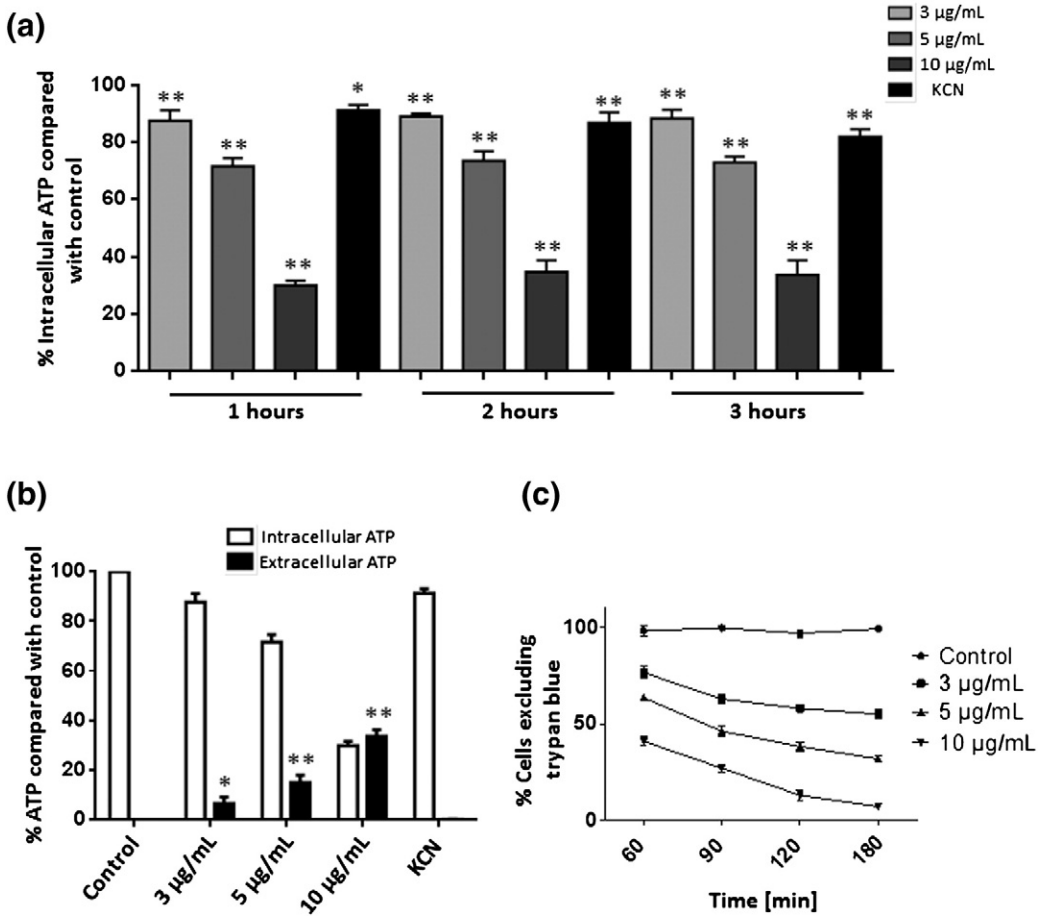

Fig. 7. The time- and concentration-dependent effect of PEI on intracellular ATP depletion and plasma membrane integrity. Panel (a) shows intracellular ATP levels following challenge with increasing concentrations of 25k-PEI-B at different time points. Cells treated with potassium cyanide (KCN, 0.5 mM) were used as a positive control. Panel (b) shows comparison of intra- and extracellular ATP levels at 1 hour incubation with 25k-PEI-B. In (a) and (b) the bars represent the mean ± SD of three parallel experiments. Statistical analyses were performed with one-way ANOVA, using Bonferroni multiple comparison correction to calculate significance ($^{*}p < 0.05$, $^{**}p < 0.01$). Panel (c) shows percentage of viable cells (based on trypan blue exclusion test) after challenge with PEI at indicated concentrations.

Additionally, subsequent PEI-mediated lysosomal membrane perturbations may also contribute to cellular stress through possible release of lysosomal cathepsins, which are endowed with the capacity to cleave Bid [3]. Likewise, a role for PEI-mediated perturbation of endoplasmic reticulum cannot be disregarded, which could also lead to energy crisis and cellular stress through activation of procaspase 12 [3]. These possibilities are currently under investigation.

In summary, this study has offered new insights as how branched PEIs could initiate mitochondrial failure and induce bioenergetic crisis through direct effect of PEI on mitochondria. Further structure–activity studies are still necessary to unravel the effect of PEI architecture and size on mitochondrial processes and energetic functions both directly and through PEI-mediated perturbation of other organelles. Indeed, a better molecular understanding of PEI-mediated mitochondrial failure events and cellular bioenergetic crisis could open the path for rational combinatorial design and construction of efficient and safer polycations (and other polymers) for nucleic acid delivery.

Competing interests

The authors declare no competing financial interests.

Acknowledgements

Financial support by the Danish Agency for Science, Technology and Innovation (Det Frie Forskningsråd for Teknologi og Produktion, reference 274-08-0534 and Det Strategiske Forskningsråd, reference 09-065746/DSF) is gratefully acknowledged.

Appendix A. Supplementary data

Supplementary data to this article can be found online at http://dx.doi.org/10.1016/j.bbabio.2013.07.001.

References

[1] H.M. Aliabadi, P. Mahdipoot, H. Uludag, Polymeric delivery of siRNA for dual silencing of Mcl-1 and P-glycoprotein and apoptosis induction in drug-resistant breast cancer cells, Cancer Gene Ther. 20 (2013) 169–177.
[2] B. Ballarin-Gonzalez, K.A. Howard, Polycation-based nanoparticle delivery of RNAi therapeutics: adverse effects and solutions, Adv. Drug Deliv. Rev. 64 (2006) 1717–1729.
[3] L. Parhamifar, A.K. Larsen, A.C. Hunter, T.L. Andresen, S.M. Moghimi, Polycation cytotoxicity: a delicate matter for nucleic acid therapy-focus on polyethylenimine, Soft Matter 6 (2010) 4001–4009.
[4] A.C. Hunter, S.M. Moghimi, Cationic carriers of genetic material and cell death: a mitochondrial tale, Biochim. Biophys. Acta Bioenerg. 1797 (2010) 1203–1209.
[5] S. Patnaik, K.C. Gupta, Novel polyethylenimine-derived nanoparticles for in vivo gene delivery, Exp. Opin. Drug Deliv. 10 (2013) 215–228.
[6] M.Y. Zheng, D. Librizzi, A. Kilic, Y. Liu, H. Renz, O.M. Merkel, T. Kissel, Enhancing in vivo circulation and siRNA delivery with biodegradable polyethylenimine-graft-polycaprolactone-block-poly(ethylene glycol) copolymers, Biomaterials 33 (2012) 6551–6558.
[7] E. Wagner, Polymers for siRNA delivery: inspired by viruses to be targeted, dynamic, and precise, Acc. Chem. Res. 45 (2012) 554–565.
[8] O. Boussif, F. Lezoualch, M.A. Zanta, M.D. Mergny, D. Scherman, B. Demeneix, J.P. Behr, A versatile vector for gene and oligonucleotide transfer into cells in culture and in vivo: polyethylenimine, Proc. Natl. Acad. Sci. U. S. A. 92 (1995) 7297–7301.
[9] A.C. Hunter, Molecular hurdles in polyfectin design and mechanistic background to polycation induced cytotoxicity, Adv. Drug Deliv. Rev. 58 (2006) 1523–1531.
[10] S.M. Moghimi, P. Symonds, J.C. Murray, A.C. Hunter, G. Debska, A. Szewczyk, A two-stage poly(ethylenimine)-mediated cytotoxicity: implications for gene transfer/therapy, Mol. Ther. 11 (2005) 990–995.
[11] P. Symonds, J.C. Murray, A.C. Hunter, G. Debska, A. Szewczyk, S.M. Moghimi, Low and high molecular weight poly(L-lysine)s/poly(L-lysine)-DNA complexes initiate mitochondrial-mediated apoptosis differently, FEBS Lett. 579 (2005) 6191–6198.
[12] D.S. Friend, D. Papahadjopoulos, R.J. Debs, Endocytosis and intracellular processing accompanying transfection mediated by cationic liposomes, Biochim. Biophys. Acta 1278 (1996) 41–50.
[13] I.S. Zuhorn, R. Kalicharan, D. Hoekstra, Lipoplex-mediated transfection of mammalian cells occurs through the cholesterol-dependent clathrin-mediated pathway of endocytosis, J. Biol. Chem. 277 (2002) 18021–18028.
[14] M.J. Reilly, J.D. Larsen, M.O. Sullivan, Polyplexes traffic through caveolae to the Golgi and endoplasmic reticulum en route to the nucleus, Mol. Pharm. 9 (2012) 1280–1290.
[15] T. Bieber, W. Meissner, S. Kostin, A. Niemann, H.P. Elsasser, Intracellular route and transcriptional competence of polyethylenimine–DNA complexes, J. Control. Release 82 (2002) 441–454.
[16] C.W. Lin, M.S. Jan, J.H.S. Kuo, L.J. Hsu, Y.S. Lin, Protective role of autophagy in branched polyethylenimine (25K)- and poly(L-lysine) (30–70K)-induced cell death, Eur. J. Pharm. Sci. 47 (2012) 865–874.
[17] G. Grandinetti, N.P. Ingle, T.M. Reineke, Interaction of poly(ethylenimine)–DNA polyplexes with mitochondria: implications for a mechanism of cytotoxicity, Mol. Pharm. 8 (2011) 1709–1719.
[18] X.L. Gao, L. Yao, Q.X. Song, L. Zhu, Z. Xia, H.M. Xia, X.G. Jiang, J. Chen, H.Z. Chen, The association of autophagy with polyethylenimine-induced cytotoxity in nephritic and hepatic cell lines, Biomaterials 32 (2011) 8613–8625.
[19] G. Kroemer, B. Dallaporta, M. Resche-Rigon, The mitochondrial death/life regulator in apoptosis and necrosis, Annu. Rev. Physiol. 60 (1998) 619–642.
[20] G.T. Babcock, M. Wikstrom, Oxygen activation and the conservation of energy in cell respiration, Nature 356 (1992) 301–309.
[21] P. Mitchell, Chemiosmotic coupling in oxidative and photosynthetic phosphorylation, Biochim. Biophys. Acta 1807 (2011) 1507–1538.
[22] Y. Hatefi, The mitochondrial electron-transport and oxidative-phosphorylation system, Annu. Rev. Biochem. 54 (1985) 1015–1069.
[23] H. Itoh, A. Takahashi, K. Adachi, H. Noji, R. Yasuda, M. Yoshida, K. Kinosita, Mechanically driven ATP synthesis by F1-ATPase, Nature 427 (2004) 465–468.
[24] D.G. Nicholls, Mitochondrial membrane potential and aging, Aging Cell 3 (2004) 35–40.
[25] P. Golstein, G. Kroemer, Cell death by necrosis: towards a molecular definition, Trends Biochem. Sci. 32 (2007) 37–43.
[26] A. Hartley, J.M. Stone, C. Heron, J.M. Cooper, A.H.V. Schapira, Complex-I inhibitors induce dose-dependent apoptosis in PC12 cells — relevance to Parkinson's disease, J. Neurochem. 63 (1994) 1987–1990.
[27] D.S. Izyumov, A.V. Avetisyan, O.Y. Pletjushkina, D.V. Sakharov, K.W. Wirtz, B.V. Chernyak, V.P. Skulachev, "Wages of fear": transient threefold decrease in intracellular ATP level imposes apoptosis, Biochim. Biophys. Acta 1658 (2004) 141–147.
[28] W. Lieberthal, S.A. Menza, J.S. Levine, Graded ATP depletion can cause necrosis or apoptosis of cultured mouse proximal tubular cells, Am. J. Physiol. 274 (1998) F315–F327.
[29] W.X. Zong, C.B. Thompson, Necrotic death as a cell fate, Genes Dev. 20 (2006) 1–15.
[30] A.K. Larsen, D. Malinska, I. Koszela-Piotrowska, L. Parhamifar, A.C. Hunter, S.M. Moghimi, Polyethylenimine-mediated impairment of mitochondrial membrane potential, respiration and membrane integrity: implications for nucleic acid delivery and gene therapy, Mitochondrion 12 (2011) 162–168.
[31] W. Pendergrass, N. Wolf, M. Poot, Efficacy of MitoTracker Green (TM) and CMXrosamine to measure changes in mitochondrial membrane potentials in living cells and tissues, Cytometry 61A (2004) 162–169.
[32] B. Ehrenberg, V. Montana, M.D. Wei, J.P. Wuskell, L.M. Loew, Membrane-potential can be determined in individual cells from the nernstian distribution of cationic dyes, Biophys. J. 53 (1988) 785–794.
[33] A.D. Presley, K.M. Fuller, E.A. Arriaga, MitoTracker Green labeling of mitochondrial proteins and their subsequent analysis by capillary electrophoresis with laser-induced fluorescence detection, J. Chromatogr. B 793 (2003) 141–150.
[34] C. Cottet-Rousselle, X. Ronot, X. Leverve, J.F. Mayol, Cytometric assessment of mitochondria using fluorescent probes, Cytometry 79A (2011) 405–425.
[35] M.D. Brand, D.G. Nicholls, Assessing mitochondrial dysfunction in cells, Biochem. J. 435 (2011) 297–312.
[36] B. Chance, G.R. Williams, Respiratory enzymes in oxidative phosphorylation. 1. Kinetics of oxygen utilization, J. Biol. Chem. 217 (1955) 383–393.
[37] E. Gnaiger, Bioenergetics at low oxygen: dependence of respiration and phosphorylation on oxygen and adenosine diphosphate supply, Respir. Physiol. 128 (2001) 277–297.
[38] D. Pesta, E. Gnaiger, High-resolution respirometry: OXPHOS protocols for human cells and permeabilized fibers from small biopsies of human muscle, Methods Mol. Biol. 810 (2012) 25–58.
[39] E. Gnaiger, Capacity of oxidative phosphorylation in human skeletal muscle: new perspectives of mitochondrial physiology, Int. J. Biochem. Cell Biol. 41 (2009) 1837–1845.
[40] C.D. Nobes, G.C. Brown, P.N. Olive, M.D. Brand, Non-ohmic proton conductance of the mitochondrial inner membrane in hepatocytes, J. Biol. Chem. 265 (1990) 12903–12909.
[41] E. Gnaiger, B. Lassnig, A.V. Kuznetsov, R. Margreiter, Mitochondrial respiration in the low oxygen environment of the cell — effect of ADP on oxygen kinetics, Biochim. Biophys. Acta 1365 (1998) 249–254.
[42] V.A. Roberts, M.E. Pique, Definition of the interaction domain for cytochrome c on cytochrome c oxidase — III. Prediction of the docked complex by a complete, systematic search, J. Biol. Chem. 274 (1999) 38051–38060.
[43] S. Matic, D.A. Geisler, I.M. Moller, S. Widell, A.G. Rasmusson, Alamethicin permeabilizes the plasma membrane and mitochondria but not the tonoplast in tobacco (*Nicotiana tabacum* L. cv Bright Yellow) suspension cells, Biochem. J. 389 (2005) 695–704.
[44] A. Berson, S. Cazanave, V. Descatoire, M. Tinel, A. Grodet, C. Wolf, G. Feldmann, D. Pessayre, The anti-inflammatory drug, nimesulide (4-nitro-2-phenoxymethanesulfoanilide), uncouples mitochondria and induces mitochondrial permeability

transition in human hepatoma cells: protection by albumin, J. Pharmacol. Exp. Ther. 318 (2006) 444–454.
[45] A. Berson, S. Renault, P. Letteron, M.A. Robin, B. Fromenty, D. Fau, M.A. Lebot, C. Riche, A.M. DurandSchneider, G. Feldmann, D. Pessayre, Uncoupling of rat and human mitochondria: a possible explanation for tacrine-induced liver dysfunction, Gastroenterology 110 (1996) 1878–1890.
[46] B.S. Mochan, W.B. Elliott, P. Nicholls, Patterns of cytochrome-oxidase inhibition by polycations, J. Bioenerg. 4 (1973) 329–345.
[47] D.S. Cafiso, Alamethicin — a peptide model for voltage gating and protein membrane interactions, Annu. Rev. Biophys. Biomol. 23 (1994) 141–165.
[48] S. Eisenhofer, F. Tookos, B.A. Hense, S. Schulz, F. Filbir, H. Zischka, A mathematical model of mitochondrial swelling, BMC Res. Note 3 (2010) 67.
[49] R.V. Benjaminsen, M.A. Mattebjerg, J.R. Henriksen, S.M. Moghimi, T.L. Andresen, The possible 'proton sponge' effect of polyethylenimine (PEI) does not include change in lysosomal pH, Mol. Ther. 21 (2013) 149–157.
[50] V.L. Gabai, A.B. Meriin, J.A. Yaglom, J.Y. Wei, D.D. Mosser, M.Y. Sherman, Suppression of stress kinase JNK is involved in HSP72-mediated protection of myogenic cells from transient energy deprivation. HSP72 alleviates the stress-induced inhibition of JNK dephosphorylation, J. Biol. Chem. 275 (2000) 38088–38094.